Investigation on CFRP as dual-functional material in chloride-contaminated solutions

Ji-Hua Zhu [a], Liangliang Wei [a], Hitham Moahmoud [b], Elena Redaelli [b], Feng Xing [a,*], Luca Bertolini [b]

[a] Guangdong Province Key Laboratory of Durability for Marine Civil Engineering, School of Civil Engineering, Shenzhen University, Shenzhen 518060, Guangdong, China [b] Politecnico di Milano, Department of Chemistry, Materials and Chemical Engineering "G.Natta", via Mancinelli, 7, 20131 Milano, Italy

This paper investigates the performance of carbon fibre reinforced polymer (CFRP) as a dual function material in combined impressed current cathodic protection and structural strengthening of reinforced concrete structures. Tests in solution showed that CFRP maintain stable electrical conductivity after 80 d accelerated anodic polarization. Results suggest that oxygen evolution occurring at low chloride ion concentration ([Cl^-]) primarily damages the carbon fibre, while chlorine evolution occurring at high [Cl^-] primarily damages the epoxy resin. The tensile strength of CFRP after anodic polarization decreases with increasing circulated charge, and, for a given circulated charge, it increases with increasing [Cl^-].

Keywords: A. Polymer - B. EIS - B. Polarization - C. Chlorination - C. Oxidation - C. Cathodic

HIGHLIGHTS

- Different polarization and [Cl^-] were considered in the accelerated testing of CFRP specimens.
- CFRP provides excellent electrical conductivity and possesses strong polarization resistance.
- The degradation of CFRP after anodic polarization was determined by two types of anode electrochemical reactions.
- The residual tensile strength of CFRP increased with increasing [Cl^-] at an equivalent degree of polarization.
- CFRP has demonstrated the practical capacity to establish multiple safeguards in an ICCP-SS system.

1. Introduction

The durability of reinforced concrete (RC) structures has been established [1], and it is generally agreed that corrosion of the embedded steel in RC is the main cause of the degradation [2,3]. Extensive investigations have been reported regarding the degradation of RC [4,5], and, among the many techniques that have been developed to prevent the corrosion of the embedded steel, impressed current cathodic protection (ICCP) has been proven to be one of the most effective [6–8], particularly in a chloride contaminated environment.

ICCP has been applied worldwide to several million square meters of RC to increase its durability [9,10]. However, while ICCP can significantly reduce the corrosion of embedded steel, it is obviously not intended to restore the load-carrying capacity of RC whose durability has deteriorated prior to the application of ICCP. To improve the load-carrying capacity of degraded RC, structural strengthening (SS) techniques using reinforcement materials such as steel plate and fibre reinforced plastic (FRP) have been developed. Unfortunately, in the absence of corrosion-oriented protection strategies such as ICCP, SS is not capable of preventing

Article history:
Received 6 August 2016
Received in revised form 23 May 2017
Accepted 28 May 2017

* Corresponding author.
E-mail address: xingf@szu.edu.cn (F. Xing).

We would like to dedicate this paper to Professor Luca Bertolini, who unfortunately passed away just after the paper was submitted for publication. Luca played an essential role in the research described here and he is greatly missed.

© 2017. This manuscript version is made available under the CC-BY-NC-ND 4.0 license http://creativecommons.org/licenses/by-nc-nd/4.0/
Published Journal Article available at http://dx.doi.org/10.1016/j.conbuildmat.2017.05.213

further corrosion of rebar in most cases. Several surveys [11,12] have reported that RC structures required further strengthening after several years because the steel reinforcement continued to suffer from active corrosion which led to enormous economic loss and resource consumption.

Considering that carbon fibre reinforced plastic (CFRP) can exchange current when it is in contact with an electrolyte, thanks to the conductivity of carbon fibres [13], a novel technique has been proposed that relies on the use of CFRP both as strengthening material and as anode for cathodic protection system [14,15]. In the present paper, this combination of ICCP and SS is defined as ICCP-SS. The ICCP-SS technique requires an affordable material with an appropriate electrical conductivity and excellent mechanical properties, both of which remain stable throughout the service life of RC, to serve as both the anode for ICCP and as the reinforcement material for SS simultaneously. From this dual perspective, carbon fibre reinforced polymer (CFRP) has been successfully applied in SS applications for RC structures [16], and, moreover, the electrical conductivity of CFRP has proven useful, particularly for damage detection of materials [17–19]. As such, CFRP appears to represent an appropriate material for serving both functions.

However, for this technique to be practicable, two fundamental and critical factors must be determined. First, the behaviour of CFRP must be determined under conditions of anodic polarization during ICCP application. Specifically, the mechanical integrity and electrochemical properties of CFRP must maintain the proper functioning of the ICCP-SS system after CFRP may suffer degradation as a result of various anodic reactions. The other critical factor to be determined is the performance of the anode interface between CFRP and concrete in the ICCP-SS system. Based on the principle of electrochemistry, the primary reaction at anode occur as Eq. (1). If in the presence of chloride, chlorine develops as Eq. (2). Indeed the interface between any type of anode material and the concrete may be critical due to possible damage of the anode or the concrete [20–24]. In the case of the combined technique considered in this paper, the bond at the CFRP/concrete interface may thus be affected by the application of ICCP. The first factor is investigated in detail in the present paper, while the CFRP/concrete interface will be discussed in future works.

$$2H_2O \rightarrow O_2 + 4H^+ + 4e^- \quad (1)$$

$$2Cl^- \rightarrow Cl_2 + 2e^- \quad (2)$$

Accelerated testing of anodes for use in concrete is commonly adopted for establishing the lifetime performance of an anode material. Unfortunately, accelerated life testing cannot be conducted in concrete because the inordinately high current levels required by the test might cause the premature anode failure owing to the electrolysis of the concrete. Therefore, accelerated life testing can be conducted in an aqueous solution, according to the NACE Standard TM0294 [25]. Accelerated tests of CFRP [14] have been conducted in three specified aqueous solutions that are used to test the ability of anodes to tolerate chlorine evolution, oxygen evolution and the actual concentrations of the pore water components. Further investigations on the failure mechanisms have been reported in [26,27]. The results indicated that CFRP is capable to be used as a dual function material for both ICCP and structural strengthening. It was also shown that degradation of CFRP in NaCl solution (chlorine evolution) is more serious than in NaOH (oxygen evolution) and pore solutions. It should be noted that a 30 g/L sodium chloride solution was used in the tests as typically adopted to test the ability of anodes to tolerate the chlorine evolution reaction. However, ICCP and structural strengthening are often used to protect various structures such as bridge piers and pilings in environments with a variety of chloride ion concentrations ([Cl^-]). It is important to investigate the dual function behaviour of CFRP in different [Cl^-] since it is no doubt that chlorine environment is one of the most important issues in the research of reinforced concrete structure durability. Hence, aqueous solutions containing chloride ions at different concentrations must be investigated to assess the performance of CFRP.

In this work, different applied current densities and [Cl^-] were considered in the accelerated testing of CFRP in solution. The feeding voltages were monitored and electrochemical impedance spectroscopy (EIS) was applied during the test period. Then, uniaxial tensile testing of CFRP was conducted, along with related microscopy analyses. An empirical equation for predicting the strength of CFRP is proposed in terms of the different types of anode electrochemical reactions expected to occur under low and high [Cl^-].

2. Experimental investigation

2.1. Preparation of CFRP specimens

CFRP is comprised of multiple layers of carbon fibres bounded by LAM-125/226 laminating epoxy (Pro-Set Inc., Bay City, MI, USA). The chemical composition of the epoxy is listed in Table 1. Each layer consists of weft-warp-knitted carbon fibres combined by the epoxy. The present study employed Toray T700 carbon fibre with a volume fraction of approximately 60% in the resulting CFRP. As shown in Fig. 1(a), CFRP specimens were fabricated into a dumbbell shape according to the ASTM-D638 standard [28] with the dimensions given in the figure. The entire surface area of each CFRP specimen was masked except for the front surface of the intermediate 35 mm × 13 mm test area (455 mm^2) for anodic polarization, as shown by the cross-sectional profile given in Fig. 1(b).

2.2. Preparation of electrolyte solutions

Electrolyte solutions with seven distinct [Cl^-] were employed for studying the influence of different concentrations on the degradation of CFRP during anodic polarization. An electrolyte solution with a fixed [Cl^-] of 1.94 wt% by weight of solution was prepared as simulated ocean water according to the ASTM-D1141 standard [29]. Solutions with reduced [Cl^-] of 0.12, 0.5, 1.0, and 1.5 wt% were prepared by diluting the standard solution, while greater concentrations of 2.5 and 3.0 wt% were prepared by adding additional sodium chloride into the standard solution. Preparation of solutions with different chloride ion concentrations is shown in Table 2.

2.3. Accelerated testing of CFRP

The accelerated testing of CFRP employed the experimental arrangement shown in Fig. 2. The circuit comprised a power supply, a CFRP anode connected to the positive terminal, a stainless steel cathode connected to the negative terminal, and an electrolyte containing the various [Cl^-]. The test solutions were refreshed every week during the 80 d period to maintain the [Cl^-] stability. The anode current density (i_{anode}) is typically limited

Table 1
Chemical composition of the epoxy employed in the CFRP specimens.

Component	Concentration (%)
Bisphenol-A type epoxy resin	37–38
Novolac epoxy resin	19–20
Dicyandiamide	5–6
Methyl ethyl ketone (MEK)	36–37

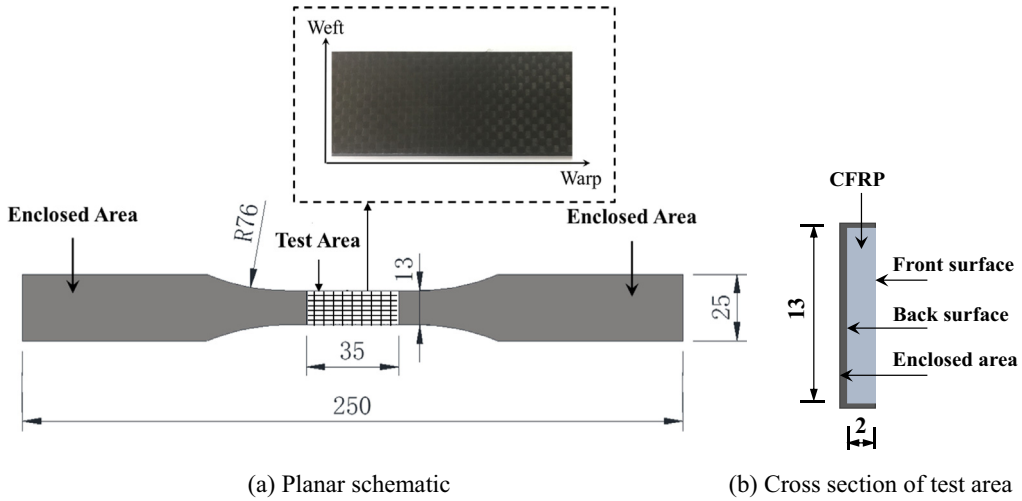

Fig. 1. Geometrical details of the CFRP specimens (mm).

Table 2
Preparation of simulated ocean water solutions with different ion concentration according to the ASTM-D1141-98 standard.

[Cl^-] wt%	Weight of component in simulated ocean water (g)										
	$MgCl_2$	Na_2SO_4	$CaCl_2$	KCl	$NaHCO_3$	KBr	H_3BO_3	$SrCl_2$	NaF	NaCl	Water
0.12	5.20	4.09	1.16	0.695	0.201	0.101	0.027	0.025	0.003	24.53	16567
0.5										24.53	3976
1.0										24.53	1988
1.5										24.53	1325
1.94										24.53	1000
2.5										34.88	1000
3.0										43.95	1000

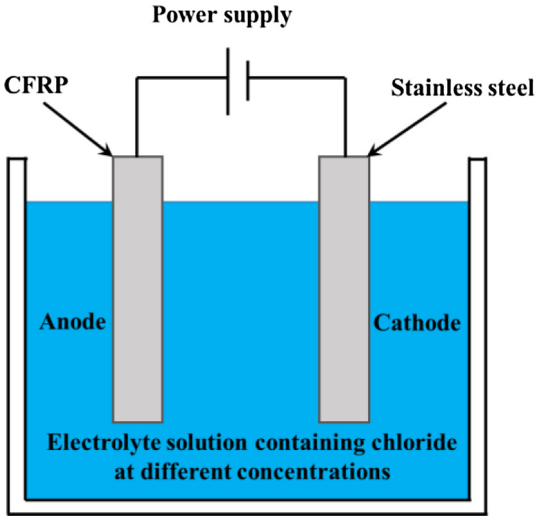

Fig. 2. Schematic view of the accelerated testing apparatus.

below 108 mA/m^2 in practical engineering design because a current density greater than this level may result in deterioration of the concrete at the anode/concrete interface [30,31]. According to the NACE Standard TM0294-2007, it requires approximately 40 years to achieve the specified charge density (38,500 A·h/m^2) of an anode if the test is operated at a current density of 108 mA/m^2. Generally, it is impossible to conduct a test program in such a long time. Therefore, this study followed the accelerated testing method by adopting large current densities in an affordable period to simulate the practical situation with smaller current densities and a rather long period. In the accelerated testing of CFRP conducted in the present study, i_{anode} of 1100 and 2200 mA/m^2, which represent respective current densities 10 and 20 times greater than the standard limiting value, were employed for studying the influence of different circulated charges on the degradation of CFRP. These anode current densities correspond to currents of 0.5 and 1.0 mA flowing into the circuit, respectively.

Three specimen groups denoted as G1, G2, and G3 were considered according to level of current supplied, given as 0.0, 0.5, and 1.0 mA, respectively. Each group was tested with seven distinct [Cl^-]. For example, the sample identified as G2(0.12) represents a sample from group 2 tested under a current of 0.5 mA within an electrolyte having a [Cl^-] of 0.12 wt%. The parameters employed in the accelerated testing of CFRP specimens are listed in Table 3. It should be noted that three replicate specimens were tested under each set of accelerated testing parameters.

2.4. Monitoring of feeding voltages, and collection of EIS data during accelerated testing

During the 80 d test period, the feeding voltages between the CFRP anode and stainless steel cathode were monitored at 5 d intervals. Moreover, EIS data was collected for the CFRP specimens on the 15th, 30th, 60th, and 80th days. The CFRP served as the working electrode, the platinum electrode served as the counter-electrode, and a saturated calomel electrode (SCE) served as the reference electrode. The applied current was interrupted, and EIS data was collected at an open circuit potential (OCP) after depolarization for 4 h. EIS data were collected over a frequency range of 100 kHz to 10 mHz [32]. A Princeton autolab-potentiostat/galvano stat Model 283 was employed for collecting EIS data, and ZSimpWin 3.10 software was employed for analysis.

Table 3
Parameters of the accelerated CFRP testing, and the results of uniaxial tensile testing.

Group	CFRP ID	i_{anode}[a] (mA/m^2)	[Cl$^-$][b] (wt%)	f_u[c] (MPa)	Failure mode[d]	δ_{Exp}[e]	δ_{Cal}[f]	$\delta_{Cal}/\delta_{Exp}$
G1	G1(0.12)	0.0	0.12	656.5	L	0.985	0.96	0.97
	G1(0.5)	0.0	0.5	653.8	L	0.981	0.96	0.98
	G1(1.0)	0.0	1.0	644.5	L	0.967	0.96	0.99
	G1(1.5)	0.0	1.5	637.8	L	0.957	0.96	1.00
	G1(1.94)	0.0	1.94	639.2	L	0.959	0.96	1.00
	G1(2.5)	0.0	2.5	632.5	L	0.949	0.96	1.01
	G1(3.0)	0.0	3.0	635.8	L	0.954	0.96	1.01
G2	G2(0.12)	1100	0.12	453.2	M	0.680	0.616	0.91
	G2(0.5)	1100	0.5	453.9	M	0.681	0.647	0.95
	G2(1.0)	1100	1.0	507.2	M	0.761	0.688	0.90
	G2(1.5)	1100	1.5	492.5	M	0.739	0.746	1.00
	G2(1.94)	1100	1.94	504.5	D	0.757	0.797	1.05
	G2(2.5)	1100	2.5	543.9	D	0.816	0.840	1.03
	G2(3.0)	1100	3.0	591.2	D	0.887	0.894	1.01
G3	G3(0.12)	2200	0.12	335.9	M	0.504	0.524	1.04
	G3(0.5)	2200	0.5	330.6	M	0.496	0.536	0.08
	G3(1.0)	2200	1.0	340.6	M	0.511	0.590	0.16
	G3(1.5)	2200	1.5	356.6	M	0.535	0.610	1.14
	G3(1.94)	2200	1.94	455.9	D	0.684	0.674	0.99
	G3(2.5)	2200	2.5	475.2	D	0.713	0.720	1.01
	G3(3.0)	2200	3.0	525.2	D	0.788	0.762	0.97
Mean								1.01
Cov[g]								0.062

[a] i_{anode} = anode current density.
[b] [Cl$^-$] = chloride ion concentration.
[c] f_u = average ultimate tensile strength of three CFRP specimens after polarization.
[d] L = lateral failure mode, D = edge delamination failure mode, M = mixed failure mode.
[e] δ_{Exp} = experimental tensile strength residual ratio, given as f_u/f_{u_RF}, where f_{u_RF} = average tensile strength of as-received CFRP (666.5 MPa).
[f] δ_{Cal} =calculated tensile strength residual ratio, given as f_{cal}/f_{u_RF}, where f_{cal} = calculated value of tensile strength of CFRP based on empirical Eq. (3).
[g] Cov = the coefficient of variation.

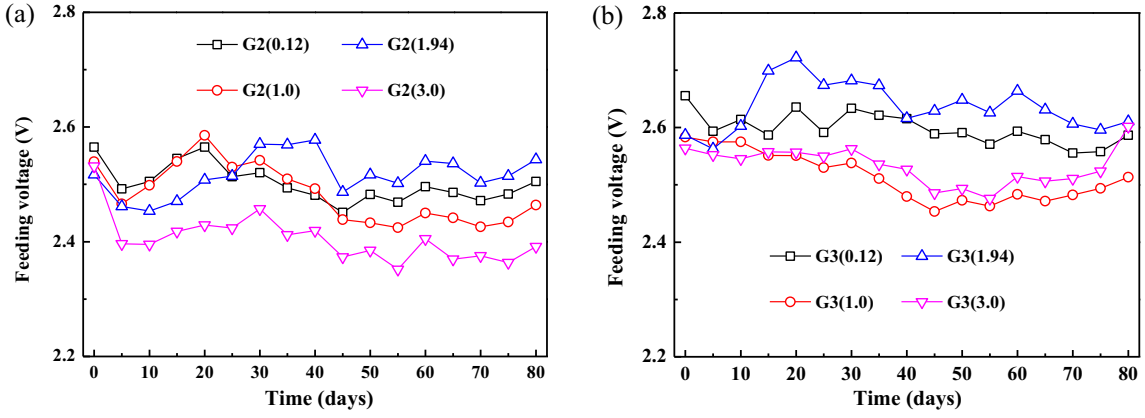

Fig. 3. Feeding voltage evolution of (a) G2 specimens and (b) G3 specimens.

2.5. Uniaxial tensile testing, and microscopy analysis of CFRP specimens after accelerated testing

After polarization for 80 d, uniaxial tensile tests of the CFRP samples were conducted on a universal test machine (E45, MTS, Eden Prairie, MN USA) with a constant loading rate of 0.1 mm/min to obtain the tensile strength of CFRP after anodic polarization. In addition, scanning electron microscopy (SEM; Hitachi S-3400 N; 15 kV accelerating voltage; ~10 mm working distance) analysis was conducted on selected CFRP specimens and a deposit obtained from an electrolyte solution. Moreover, energy dispersive spectroscopy (EDS, Hitachi S-3400 N) was conducted for the deposit sample.

3. Experimental results

3.1. Feeding voltage

Fig. 3(a) and (b) show the evolution of the feeding voltages between CFRP and stainless steel electrodes for G2 and G3 specimens, respectively, during accelerated testing for 80 d, for selected [Cl$^-$]. The results indicate that the feeding voltages maintained stable values with minor fluctuations of 100 mV. A slight decrease in the feeding voltages was observed in the first week, which then generally increased to a maximum value that remained fairly constant until the end of the test. The feeding voltages fluctuated around average values of approximately 2.5 and 2.6 V for anode current densities of 1100 and 2200 mA/m^2, respectively. The feeding voltages of the G3 specimens were similar to those of the G2 specimens even though the G3 specimens were subjected to a current that was twice that of the G2 specimens. This is most likely attributable to the CFRP/electrolyte interface, which works as a capacitor rather than as a resistance [33].

These results demonstrate that the feeding voltage of the circuit is not greatly influenced by the applied current and the [Cl$^-$]. It is shown that CFRP maintain stable electrical conductivity after 80 d anodic polarization in the test environments.

3.2. Tensile test of CFRP after polarization

Fig. 4 depicts the three failure modes obtained from uniaxial tensile testing of CFRP specimens after anodic polarization. Fig. 4(a) depicts lateral failure (denoted as L) across the gauge length of the specimen. Fig. 4(b) depicts vertical failure along the specimen with edge delamination (denoted as D). Fig. 4(c) depicts mixed failure (denoted as M), combining lateral and vertical failures.

Table 3 lists the failure modes observed for specimens subjected to each set of accelerated testing parameters. It is observed that all G1 specimens exhibited the L failure mode, which is the typical failure of as-received CFRP. The G1 specimens were clearly not degraded seriously due to exposure to chloride solution without polarization. In addition, G2 and G3 specimens subjected to relatively low [Cl^-] (0.12–1.5 wt%) exhibited the M failure mode while those with greater [Cl^-] (1.94–3.0 wt%) exhibited the D failure mode. This is most likely attributable to different degradation mechanisms of CFRP when immersed in different [Cl^-] under polarization. Further investigation is presented in Section 4 of the present paper.

The mechanical performance of CFRP specimens obtained from uniaxial tensile tests after polarization is shown in Fig. 5. The average tensile strength of as-received CFRP (f_{u_RF}) was 666.5 MPa. The tensile strength residual ratio (δ_{Exp}) is the ratio of the tensile strength of tested CFRP (f_u) to f_{u_RF}, the results of which are listed in Table 3, where the average values of the three specimens subjected to the accelerated testing under equivalent conditions are given. Here, a value lower than 1 represents a decrease of the tensile strength of CFRP specimens with respect to as-received. The results clearly show that δ_{Exp} decreased with increasing applied current for each [Cl^-]. For a [Cl^-] of 0.12 wt%, δ_{Exp} = 0.985 for G1(0.12) while δ_{Exp} = 0.680 for G2(0.12) and δ_{Exp} = 0.504 for G3(0.12). For a [Cl^-] of 3.0 wt%, δ_{Exp} = 0.954 for G1(3.0) whereas δ_{Exp} = 0.887 for G2(3.0) and δ_{Exp} = 0.788 for G3 (3.0). Fig. 5 also demonstrates that the [Cl^-] significantly affects the value of δ_{Exp} for an equivalent applied current. In the absence of polarization, the values of δ_{Exp} for the G1 specimens decreased slightly with increasing [Cl^-], ranging from 0.949 to 0.985. The values of δ_{Exp} for both the G2 and G3 specimens increased with increasing [Cl^-], where δ_{Exp} = 0.680 for G2(0.12) in comparison to δ_{Exp} = 0.887 for G2(3.0), and δ_{Exp} = 0.504 for G3(0.12) compared with δ_{Exp} = 0.788 for G3(3.0).

These experimental results indicate that the tensile strength of CFRP after polarization was influenced by a synergetic effect involving anodic polarization and chloride ions. The results demonstrate that the CFRP samples subjected to relatively low [Cl^-] suffered more severe degradation than when subjected to greater [Cl^-] at the same polarization.

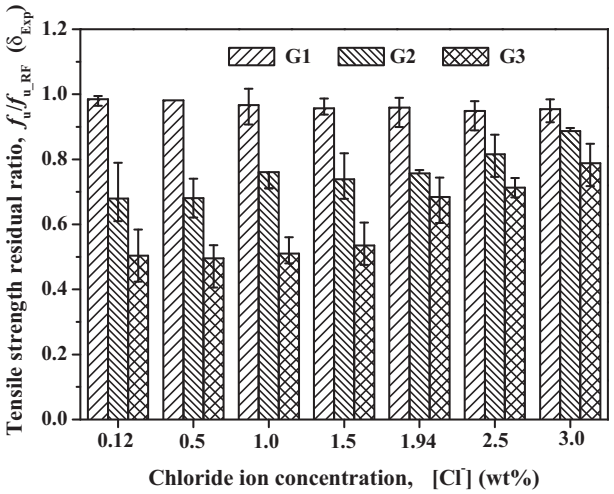

Fig. 5. Tensile strength residual ratio (δ_{Exp}) of CFRP specimens tested in electrolyte solutions containing different [Cl^-].

4. Investigation of the degradation of CFRP after anodic polarization

4.1. EIS analysis of CFRP

The degradation of CFRP specimens is intimately connected with the electrochemical reactions occurring on the surface of the anode, the detailed analysis of which EIS is imminently well suited. Fig. 6(a, b), (c, d), and (e, f) respectively present Bode plots of G1, G2, and G3 CFRP specimens in electrolyte solutions containing different [Cl^-] at the 30th and 80th polarization stages. The displayed data indicated that, when no current regime was applied, the overall impedance was relatively higher in case of G1 samples than in case of G2 and G3 samples, as shown in Fig. 6(a, b), (c, d), and (e, f), respectively. Furthermore, a slight decrease in the impedance magnitude |Z|, particularly in the high frequency domain, was observed when increasing the [Cl^-] in the electrolyte, and this trend was accentuated by ageing, as shown in Fig. 6(b). However, Fig. 6(c)–(f) show substantial variations in the impedance response owing to the synergetic effect of applied current density and [Cl^-]. The values of |Z| measured at low frequency decreased by two orders of magnitude after 80 d of applying currents of 0.5 and 1.0 mA (Fig. 6(d) and (f)) for different [Cl^-].

To have more information about different electrochemical processes occur during polarization regime of CFRP at different exposure conditions, the fitting parameters of EIS response were considered. The best-fit of the time constants in the EIS spectra were fitted using the electrochemical equivalent circuit (EEC) shown in Fig. 7. The modulus of the maximum phase angle in all EIS spectra was less than 90°, as shown in Fig. 6, and such behaviour can be interpreted as a deviation from ideal capacitor behaviour. Deviation of this nature has been denoted as frequency dispersion, which has been attributed to inhomogeneity in the dielectric material, porosity, mass transport, and a relaxation effect [34]. Therefore, in the proposed EEC, constant phase elements (Q_n, n = 1, 2, units: Ω^{-1} cm^{-2} s^{α}, for $0 \leq \alpha \leq 1$) were employed to fit the high and medium time constants in conjunction with resistances

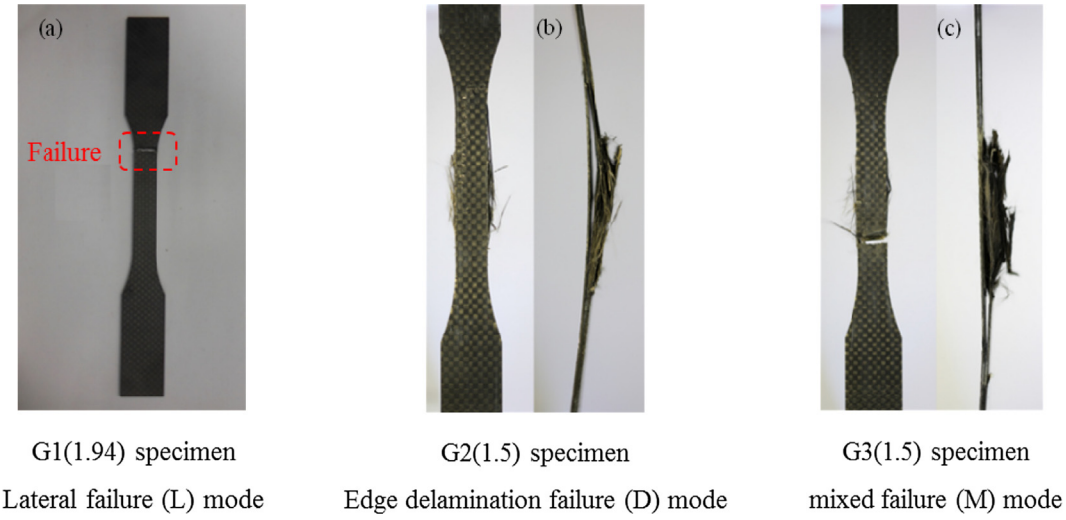

Fig. 4. Failure modes of CFRP specimens obtained from uniaxial tensile tests: (a) G1(1.94) specimen, lateral failure (L) mode; (b) G2(1.5) specimen, edge delamination failure (D) mode; and (c) G3(1.5) specimen, mixed failure (M) mode.

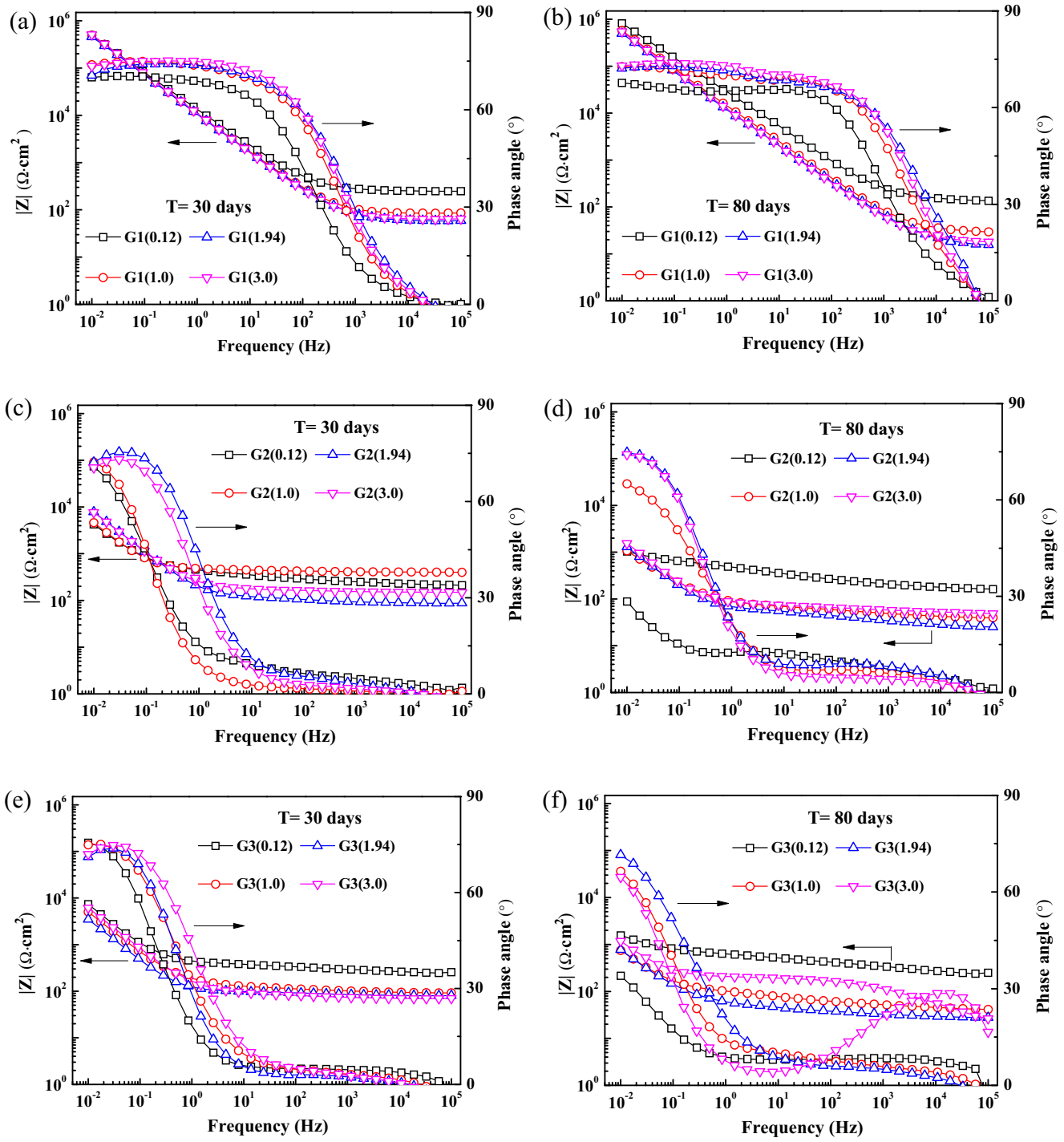

Fig. 6. Bode plots of CFRP specimens in electrolyte solutions containing different [Cl^-] at various polarization stages: G1 specimens at the (a) 30th and (b) 80th days; G2 specimens at the (c) 30th and (d) 80th days; and G3 specimens at the (e) 30th and (f) 80th days.

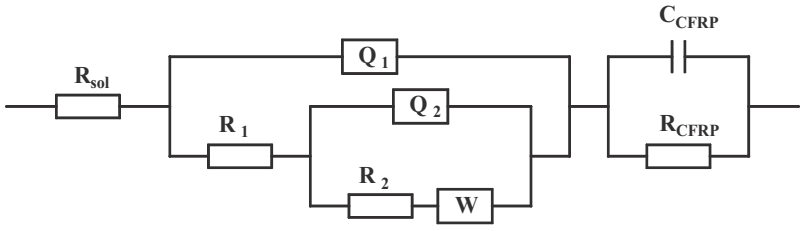

Fig. 7. Equivalent circuit used to model the experimental EIS data collected for CFRP electrodes.

R_n. The EIS data fitting were performed by using three time constants, the high and medium time constants (R_1Q_1 and R_2Q_2) were mainly related to the electrochemical processes occurred on the anode/electrolyte interface, and the low frequency time constant was associated to the redox processes occurred in the CFRP anodes. For the high frequency time constant (R_1Q_1), R_1 represents the interfacial electrolyte resistance. The R_2Q_2 time constant was correlated to the active CFRP surface, and it was represented by a charge transfer resistance (R_2) and an admittance associated with the double layer capacitance. A Warburg impedance W is added for modelling the diffusion of ionic species at the CFRP/electrolyte interface. The low frequency time constant parameters are given as R_{CFRP} and C_{CFRP} that related to the CFRP resistance and corresponding capacitance. Finally, the solution resistance is given as R_{sol}.

The evolution of R_2 and the double layer capacitance (C_2) calculated from Q_2 according to the expression $C = Q^{1/\alpha}\ R^{(1-\alpha)/\alpha}$, for $\alpha = 0.5 \rightarrow 1$ [35], for G1, G2, and G3 specimens are shown in Fig. 8. The displayed data in Fig. 8(a) indicate that, in the absence of applied current regime, a remarkable decrease in C_2 values was monitored for all G1 specimens by ageing. This decrease in C_2 values with ageing suggest a less CFRP surface activation, even in presence of different chloride content. After 15 days, C_2 varied depending on [Cl^-], however, after 60 days, no clear effect of [Cl^-] on C_2 values was deduced in case of G1 specimens. On the other side, the charge transfer resistance R_2 values were slightly affected by [Cl^-]: in early ages (after 15 days), the R_2 values measured in low chloride content, 0.12 and 1.0 wt%, were relatively higher than in case of high chloride content solutions (1.94 and 3.0 wt%), see Fig. 8(a). Thereafter, the R_2 values of CFRP immersed solutions with 0.12 and 1.0 wt% decreased by ageing, while R_2 values in case of 1.94 and 3.0 wt% solutions slightly increased, reaching nearly the same R_2 values after 80 days, which in turn indicated that [Cl^-] exhibited no distinguishable effect on G1-CFRP specimen, in agreement with measured C_2 values at the same exposure time.

Nevertheless, for G2 and G3 specimens, CFRP showed different electrochemical response, mainly because of the dual effect of the applied current densities and the chloride content. For G2 and G3 specimens, higher C_2 values than in case of G1 specimens were measured at the same immersion time. Moreover, C_2 of G2 and G3 specimens tends to increase with ageing, Fig. 8(b) and (c). The evolution of R_2 parameter for G2 and G3 specimens concluded that, in accordance to C2 values, R_2 tends to decrease in most cases by ageing till 60 days. This decrease in R_2 values was maintained after 80 days for G2 specimens with relatively low [Cl^-] (i.e. 0.12 and 1.0 wt%), Fig. 8(b), while for G3 specimens, R_2 values increased after 80 days, Fig. 8(c), which probably related to carbon fibre and epoxy damage and formation of voids in G3 specimens after 80 days formed on the outer fibre surface [36].

The variation in the double layer capacitance and charge transfer resistance is mainly related to the active part of the surface. Therefore, changes in these parameters reflect changes in the active surface area of the CFRP. The probable reason for increased CFRP surface activation in electrolyte solutions with low [Cl^-], especially in case of G2 specimens, is the induced electrochemical oxidation of CFRP by the oxygen evolution process. In this case, CFRP surface activation increases with an increasing applied current density, as can be deduced from Fig. 8(b). However, in electrolyte solutions with greater [Cl^-], chlorine evolution becomes a predominate process. Consequently, a reduction in the electrochemical oxidation of CFRP is expected. In case of high current densities (i.e. G3 specimens), depending on [Cl^-], both oxygen and chloride evolution are expected after 80 days, Fig. 8(c).

Fig. 9 shows the variation in R_{CFRP} and C_{CFRP} with respect to exposure time. The time constant $R_{CFRP}C_{CFRP}$ is primarily related to processes occurring inside the CFRP electrode. The results in Fig. 9 indicate that, $R_{CFRP}C_{CFRP}$ time constant showed similar variation trends to R_2C_2 times constant was observed, which can be attributed to a possible overlapping between the middle and low frequency time constants. The displayed data for G1 specimens, Fig. 9(a), indicated that, C_{CFRP} tends to decrease with ageing, moreover, a clear increase in C_{CFRP} with increasing [Cl^-] during earlier time intervals were reported. Besides, during 60 days of immersion, R_{CFRP} increased with ageing time. During this period, a relatively higher R_{CFRP} values of G1 specimens in low [Cl^-] (i.e., 0.12 and 1.0 wt%) was measured. However, after 80 days of immersion, nearly the same R_{CFRP} and C_{CFRP} was registered, Fig. 9(a).

Regarding the variation in R_{CFRP} and C_{CFRP} parameters in case of G2 and G3 specimens, the data shown in Fig. 9(b) and (c) reveal that both R_{CFRP} and C_{CFRP} increased with immersion time when dif-

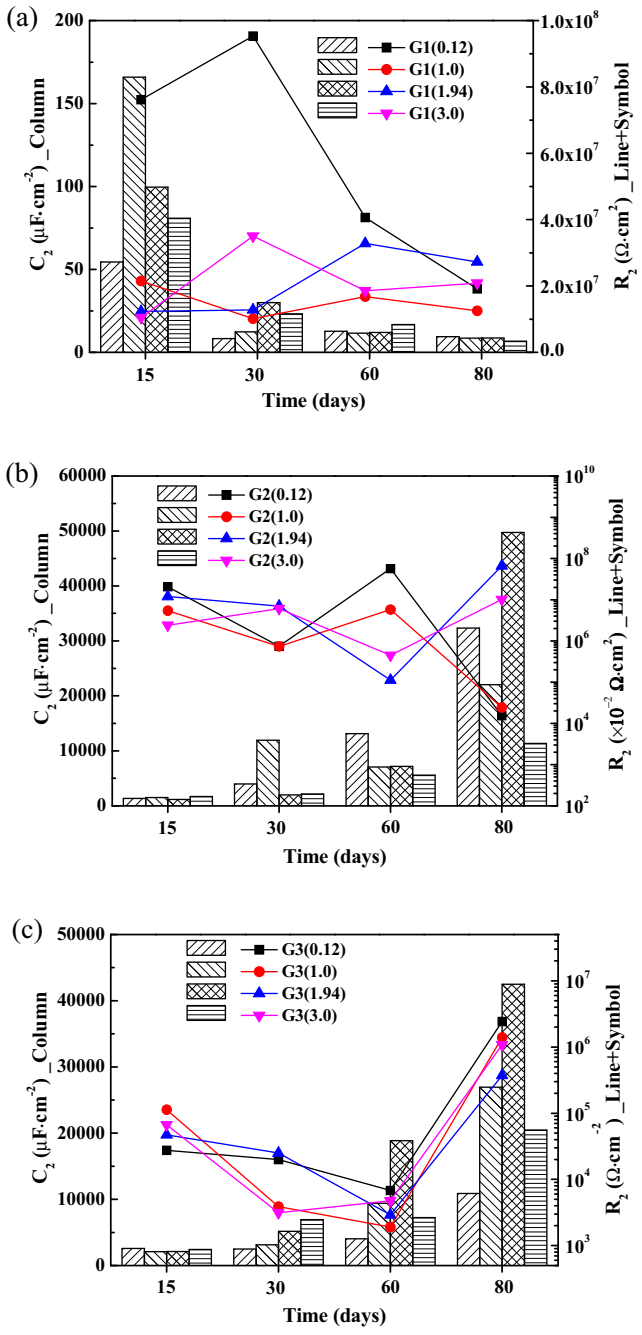

Fig. 8. Evolution of the charge transfer resistance (R_2) and the double layer capacitance (C_2) based on the equivalent circuit model given in Fig. 7: (a) G1 specimens; (b) G2 specimens; and (c) G3 specimens.

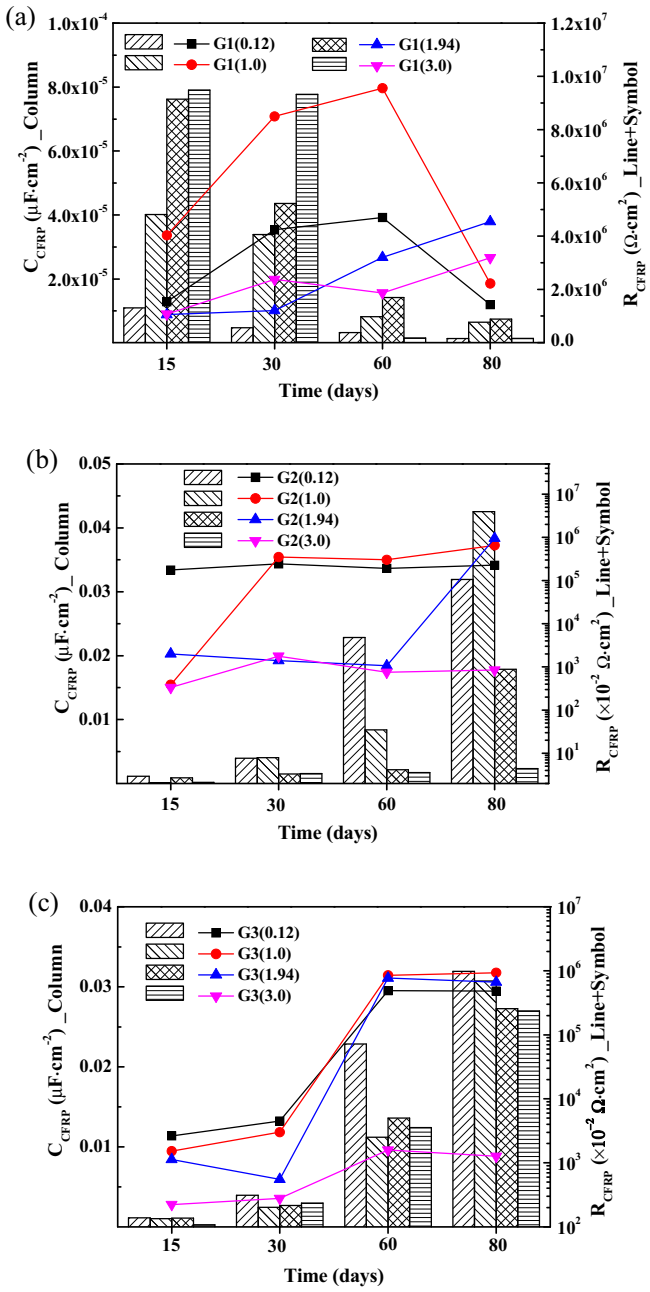

Fig. 9. Evolution of the low frequency time constant parameters, R_{CFRP} and C_{CFRP}, based on the equivalent circuit model given in Fig. 7: (a) G1 specimens; (b) G2 specimens; and (c) G3 specimens.

ferent current densities were applied. The comparison of R_{CFRP} and C_{CFRP} parameters after 80 days for G2 and G3 specimens, Fig. 9 (b) and (c), indicated that, the higher is the chloride content, the lower is C_{CFRP} value. Additionally, the highest R_{CFRP} values we obtained for CFRP when the [Cl^-] are less than 3.0 wt% for G2 and G3 specimens. This increase in R_{CFRP} and C_{CFRP} in low [Cl^-] electrolytes suggests a decrease in the interfacial adhesion between the carbon fibre and epoxy resin, which appears to be more evident at larger current densities and increased ageing.

The interfacial adhesion between the carbon fibre and epoxy is determined by the reaction between oxygen-containing function groups on the carbon fibre (primarily the carboxyl group, which is known to be an acidic carbon fibre group) and epoxy hydroxyl groups [37,38]. For electrolytes with relatively low [Cl^-], the applied current densities are likely to have affected the chemical bonding between the carbon fibre acidic group and the epoxy resin, which can induce the formation of a micropore/void/slit structure, and this structure could increasingly progress toward the anode interior from the outer fibre surface with increasing applied current density [37].

The various electrochemical reactions occurring on the anode result in different levels of degradation to the carbon fibre and epoxy resin. In electrolytes with greater [Cl^-] solutions, an abundance of chloride is located in the vicinity of the CFRP anode such that chlorine evolution becomes predominate process, resulting in decomposition of the epoxy resin. However, in electrolytes with relatively low [Cl^-], oxygen evolution prevails chlorine evolution as the number of chloride ions are reduced at the CFRP/electrolyte interface, and the carbon fibre is dissolved under the process of oxygen evolution.

4.2. Microscopy analysis of electrolyte deposits and CFRP samples after polarization

As shown in Fig. 10, the colour of the electrolyte solutions exhibited substantial variation after accelerated testing of CFRP depending upon the charge densities and [Cl^-] employed. The electrolyte solutions for G1 specimens (Fig. 10(a)) remained transparent, whereas the solutions for G2 and G3 specimens (Fig. 10 (b) and (c)) exhibited colours that varied from heavy black to light yellow with increasing [Cl^-] that indicates different electrochemical reactions occurred on CFRP.

In addition to solution colour variation, some black deposits were observed on the bottom of the electrolyte solution vessels. These black deposits were collected from the solution of G3(0.12) specimens, filtered and dried for examination by SEM. Fig. 11(a) presents an SEM micrograph with the elements identified by EDS in Fig. 11(b). The black deposit is observed to exhibit a honeycomb texture, and a great quantity of C is observed within detecting area A.

Fig. 12(a) shows the SEM image that the carbon fibre has been encapsulated overall by the epoxy resin in a reference CFRP. Fig. 12(b) and (c) respectively present SEM micrographs indicative of the surface morphology of G3(0.12) and G3(3.0) after anodic polarization for 80 d, which are respectively representative of low and high [Cl^-]. In the case of the lower [Cl^-], a fairly substantial amount of epoxy resin is observed to cover the carbon fibres. In contrast, the greater [Cl^-], the epoxy resin was largely dissolved while the carbon fibre maintained its integrity. Studies have demonstrated a relationship between the consumption of a graphite anode and the electrochemical reactions occurring on the anode surface, where the rate of consumption was reported as about 0.9 kg/A per year when oxygen evolution was dominant while the rate was 0.14–0.23 kg/A per year when chlorine evolution was dominant [39]. This supports the hypothesis that oxygen evolution in relatively low [Cl^-] principally attacks the carbon fibre while chlorine evolution in greater [Cl^-] primarily damages the epoxy resin. It can be assumed from these observations that the black deposits derived from the carbon fibre of the CFRP anode.

In summary, it has been found that the chlorine evolution occurred firstly in the chloride-contaminated environment, which will damage the resin of CFRP. However, the oxygen evolution would be activated when the chloride content is lower or/and the applied current density is high enough [3]; in this case, it is the carbon fibres of CFRP that is mainly damaged. Meanwhile, it has been well-known that the strength of CFRP is mainly from carbon fibres. Theoretically, the strength of CFRP from the former case should be higher than that from the latter case. This is coincident with the experiment results obtained from the tensile tests of CFRP after polarization.

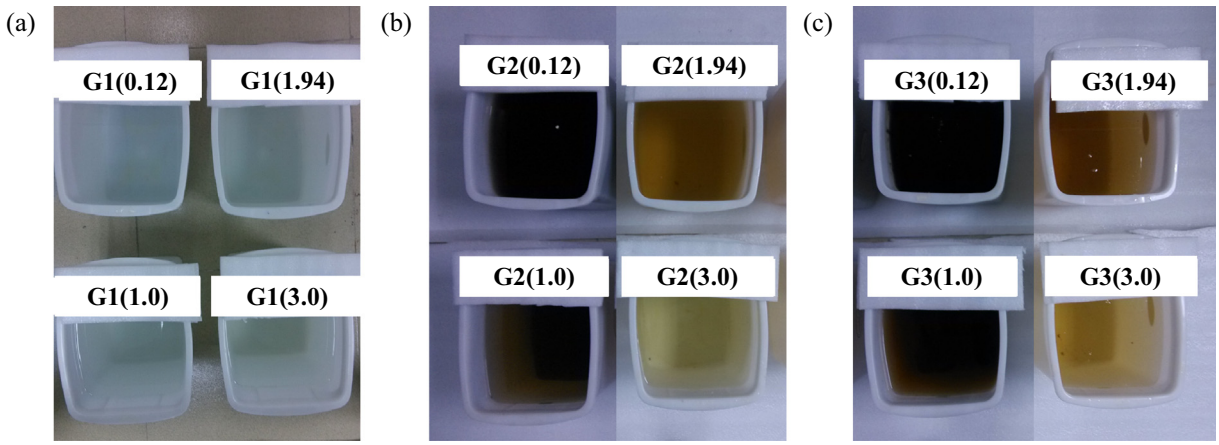

Fig. 10. Electrolyte solution colour after 80 d for (a) G1 specimens, (b) G2 specimens, and (c) G3 specimens after polarization.

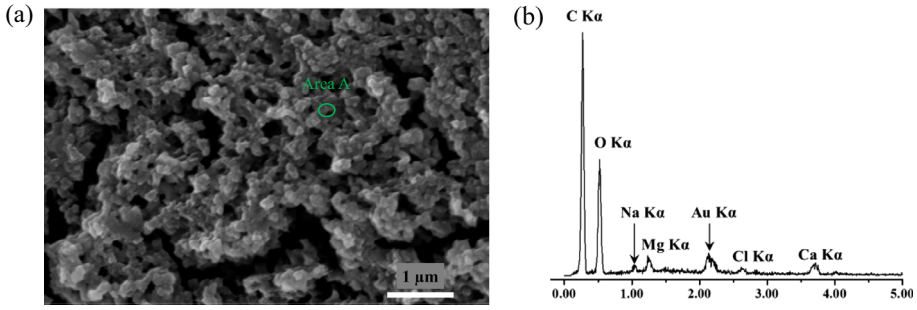

Fig. 11. SEM micrograph of a black deposit obtained from an electrolyte solution after polarization: (a) surface morphology; and (b) EDS spectrum of the elements observed at Area A given in (a).

5. Strength of CFRP after anodic polarization

The strength of CFRP after the anodic polarization process conducted has been shown to be determined by the synergetic effect of the applied current and the [Cl^-]. The circulated charge density was here adopted to quantify the effect of applied current density in time. The data markers in Fig. 13 present the values of δ_{Exp} (also given in Table 3) for CFRP specimens subjected to anodic polarization in different [Cl^-] environments. The strength of CFRP is observed to decrease with increasing charge density, and it also decreases with decreasing [Cl^-] at a given circulated charge. This effect of [Cl^-] is consistent with the different CFRP degradation mechanisms, oxygen evolution in the carbon fibre at relatively low [Cl^-] and chlorine evolution in the epoxy resin at greater [Cl^-]. Based on these results, an empirical equation can be proposed, as shown in Eq. (3), to predict the residual tensile strength of CFRP after anodic polarization at a given charge density for relatively low and greater [Cl^-], respectively.

$$f_u = \delta f_{u\_RF} \tag{3}$$

where,

$$\delta = f(q) f([Cl^-]) \tag{3-1}$$

$$f(q) = -1.2 \times 10^{-4} \times q + 1.425 \quad 0 < q < 4224 Ah/m^2 \tag{3-2}$$

$$f([Cl^-]) = \begin{cases} 0.04 \times [Cl^-] + 0.58, & [Cl^-] : 0.12 - 1.5\ wt\% \\ 0.11 \times [Cl^-] + 0.5, & [Cl^-] : 1.94 - 3.0\ wt\% \end{cases} \tag{3-3}$$

where f_u = tensile strength of CFRP after anodic polarization, $f_{u\text{-}RF}$ = tensile strength of reference CFRP without polarization, q = the circulated charge density, δ = tensile strength residual ratio, [Cl^-] = chloride ion concentration.

Fig. 14 compares the experimental and calculated data against the chloride ion concentrations. Table 3 also summarizes the experimental tensile strength residual ratio (δ_{Exp}) obtained from the presented test program against the calculated values (δ_{Cal}) based on Eq. (3). The mean value and the coefficient of variation (Cov) of the $\delta_{Cal}/\delta_{Exp}$ ratios are 1.01 and 0.062, respectively, which demonstrates that the equation can be employed to accurately predict the tensile strength of CFRP after anodic polarization in different [Cl^-].

6. Performance of CFRP in ICCP-SS

In the present study, CFRP was subjected to accelerated polarization under a maximum current density of 2200 mA/m^2 for 80 d. At the end, the total charge density passed during the test was 4224 A·h/m^2. The tensile strength of CFRP decreased in the testing environment and the most serious loss of tensile strength was obtained for specimen G3(0.5) with the δ_{Exp} of 0.496. A large number of research [40–42] have shown that, when CFRP is applied for structural strengthening of reinforced concrete structures, the utilization efficiency of the tensile strength of CFRP ranges from 45 to 75%. In the present work, when CFRP supplied the maximum charge density of 4224 A·h/m^2, it was still within those threshold values, and hence it can be assumed that it was capable of serving as both the anode for ICCP and as the reinforcement material for SS simultaneously.

Accelerated polarization tests were adopted in the present study with the current densities much larger than the practical value. Since the performance of CFRP has been demonstrated with

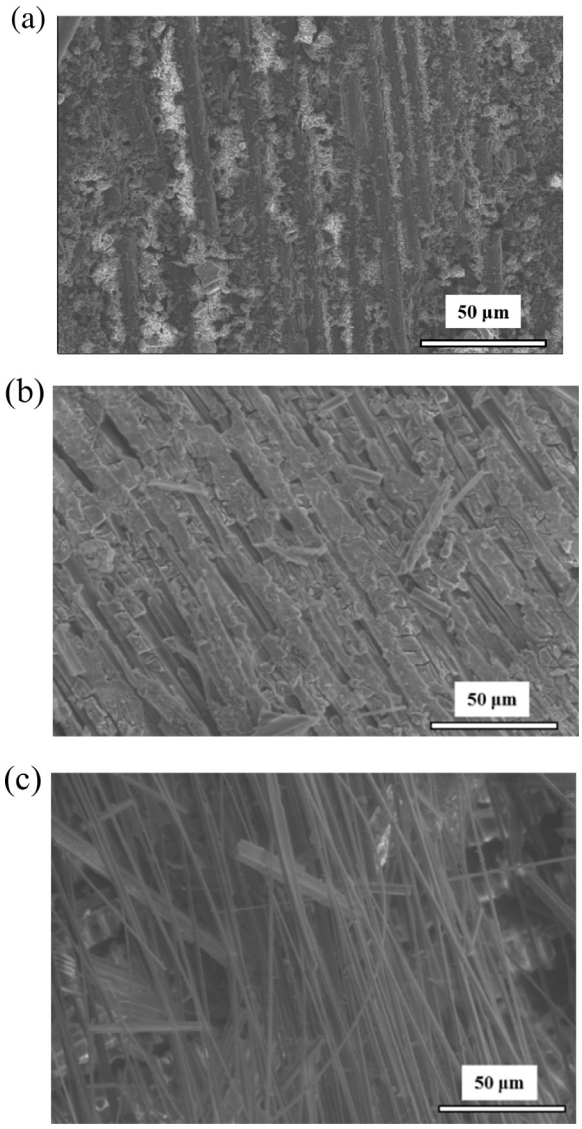

Fig. 12. SEM images of (a) a reference CFRP (b) G3(0.12) and (c) G3(3.0) after anodic polarization.

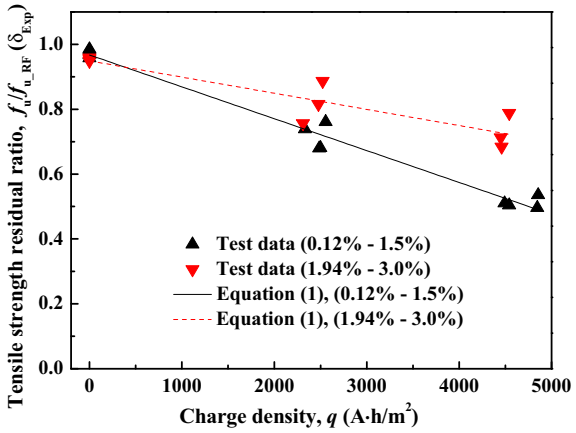

Fig. 13. Experimental tensile strength residual ratio (δ_{Exp}) values obtained from Table 3 (given by the data markers) for CFRP after anodic polarization at different [Cl$^-$] environments along with calculated values based on Eq. (3).

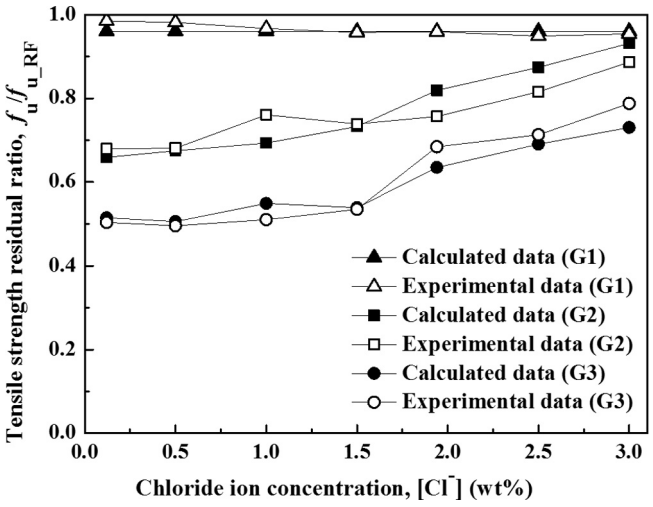

Fig. 14. Comparison of experimental and calculated tensile strength residual ratios against the chloride ion concentrations.

the total charge density up to 4224 A·h/m^2, the service life of CFRP in an ICCP-SS system can be calculated based on the equilibrium of charge quantity between the cathode ($Q_{cathode}$) and anode (Q_{anode}), as detailed in [14]. The calculation is based on a typical layout of RC structures with a number of steel reinforcing bars (n) and the CFRP wrapping around, where the CFRP and the steel bars serve as the anode and the cathode, respectively. By assuming that Q_{anode} = 4224 A·h/m^2 is the governing value, the service life of the CFRP can be predicted according to the Eq. (4).

$$Q_{anode} = Q_{cathode} = n \times A_{steel} \times i_{cathode} \times t_{life} = i_{cathode} t_{life} \sqrt{4\pi n A_c \rho} \quad (4)$$

where: n = number of steel bars; A_{steel} = surface area of steel reinforcements of unit length in contact with concrete; $i_{cathode}$ = applied protection current density of cathode (steel); A_c = cross-sectional area of concrete element; ρ = reinforcement ratio of concrete element, which can be calculated by dividing the cross-sectional area of concrete by the total cross-sectional area of steel reinforcements in concrete; t_{life} = service life of CFRP in an ICCP-SS system governed by Q_{anode}.

Therefore, for a concrete element with a cross-section of 400 × 400 mm^2 and n = 8, the service life of CFRP is more than 40 years, even with the maximum standard limiting values of $i_{cathode}$ = 20 mA/m^2 and ρ = 5%, respectively. It should be observed that 40 years is an acceptable service life for an anodic system and thus results shown in this work suggest that ICCP-SS may be an interesting approach for combined strengthening and corrosion protection of RC structures esposed to chloride environments. Nevertheless, it should be emphasised that the service life of an ICCP-SS is not only determined by the performance of CFRP laminate itself, as discussed in the introduction of the present paper but also by the CFRP-concrete interface and the material used for bonding. Further investigations on the performance of the CFRP anode applied to simulated concrete elements are still necessary before practical rules for the applications of the ICCP-SS can be proposed.

7. Conclusions

The present paper investigated the electrochemical and mechanical performances of CFRP for use in a proposed ICCP-SS system. Different applied current and [Cl$^-$] were considered in the process of accelerated testing of CFRP specimens in solutions. A variety of analysis methods and mechanical measurements were

conducted during and after accelerated testing. Based on the experimental results and related discussion, the following conclusions can be drawn.

1. The feeding voltage of the circuit employing CFRP as an anode in solution was not greatly influenced by the circulated charges and [Cl^-]. It is shown that CFRP maintain stable electrical conductivity after 80 d anodic polarization in the test environments.
2. The tensile strength residual ratio decreased slightly with increasing [Cl^-] without polarization, and also decreased with an increasing circulated charge at an equivalent [Cl^-], whereas it increased with increasing [Cl^-] at an equivalent circulated charge.
3. The degradation of CFRP after anodic polarization was determined by two types of anode electrochemical reactions, which are oxygen evolution and chlorine evolution. Oxygen evolution primarily resulted in carbon fibre damage, and chlorine evolution primarily resulted in epoxy resin damage. The tensile strength of CFRP decreased to a greater extent owing to oxygen evolution than as a result of chlorine evolution.
4. An empirical equation was proposed to predict the tensile strength of CFRP after anodic polarization in electrolyte solutions containing different [Cl^-].
5. Even at high anodic polarization with the charge density up to 4224 $A{\cdot}h/m^2$, CFRP has demonstrated the practical capacity to establish multiple safeguards by maintaining sufficient strength and stable electrochemical response over an extended duration in an ICCP-SS system.

Acknowledgements

The research work described in this paper was supported by the Chinese National Natural Science Foundation (Project No. 51538007, 51478269) and the European Research Council (Project No. FP7-PEOPLE-2011-IRSES-294555_DOSECOPS).

References

[1] P.K. Mehta, Concrete durability-fifty years progress, in: Proceedings of the 2nd International Conference on Concrete Durability, Montreal, QC, Canada, 1991, p. 132.
[2] Y. Zhao, J. Yu, W. Jin, Damage analysis and cracking model of reinforced concrete structures with rebar corrosion, Corros. Sci. 53 (2011) 3388–3397.
[3] L. Bertolini, B. Elsener, P. Pedeferri, E. Redaelli, R. Polder, Corrosion of Steel in Concrete: Prevention, Diagnosis, Repair, 2nd ed., Wiley-VCH, Weinheim, 2013.
[4] C.G. Berrocal, I. Löfgren, K. Lundgren, L. Tang, Corrosion initiation in cracked fibre reinforced concrete: influence of crack width, fibre type and loading conditions, Corros. Sci. 98 (2015) 128–139.
[5] Y. Zhao, J. Dong, Y. Wu, H. Wang, X. Li, Q. Xu, Steel corrosion and corrosion-induced cracking in recycled aggregate concrete, Corros. Sci. 85 (2014) 241–250.
[6] P. Pedeferri, Cathodic protection and cathodic prevention, Constr. Build. Mater. 10 (1996) 391–402.
[7] R.B. Polder, W.H.A. Peelen, F. Lollini, E. Redaelli, L. Bertolini, Numerical design for cathodic protection systems for concrete, Mater. Corros. 60 (2009) 130–136.
[8] C. Christodoulou, G. Glass, J. Webb, S. Austin, C. Goodier, Assessing the long term benefits of Impressed Current Cathodic Protection, Corros. Sci. 52 (2010) 2671–2679.
[9] H.B. Gao, B.Y. Liu, Application of Impressed Current Cathodic Protection System (ICCP) to Offshore Wind Farms, Corros. Protect. 34 (2013) 1108–1110.
[10] ASTM STP1370, Design of impressed current cathodic protection (ICCP) systems for U.S. Navy Hulls, 1999.
[11] P. Balaguru, A. Nanni, J. Giancaspro, FRP Composites for Reinforced and Prestressed Concrete Structures: A Guide to Fundamentals and Design for Repair and Retrofit, Taylor & Francis, 2009.
[12] G. Malumbela, M. Alexander, P. Moyo, Serviceability of corrosion-affected RC beams after patch repairs and FRPs under load, Mater. Struct. 44 (2011) 331–349.
[13] L. Bertolini, M. Gastaldi, M.P. Pedeferri, Risk of galvanic corrosion induced by CFRP strengthening in reinforced concrete, in: M. Raupach, B. Elsener, R. Polder, J. Mietz (Eds.), Corrosion of Reinforcement in Concrete: Monitoring, Prevention and Rehabilitation Techniques, Woodhead Publishing Limited, Cambridge, 2007, pp. 62–74.
[14] J.H. Zhu, M. Zhu, N. Han, W. Liu, F. Xing, Electrical and mechanical performance of carbon fiber-reinforced polymer used as the impressed current anode material, Materials 7 (2014) 5438–5453.
[15] P. Lambert, C. Van Nguyen, P.S. Mangat, F.J. O'Flaherty, G. Jones, Dual function carbon fiber fabric strengthening and impressed current cathodic protection (ICCP) anode for reinforced concrete structures, Mater. Struct. 48 (2015) 2157–2167.
[16] ACI 400, Guide for the design and construction of externally bonded FRP systems for strengthening concrete structures, 2003.
[17] M. Kupke, K. Schulte, R. Schüler, Non-destructive testing of FRP by d.c. and a.c. electrical methods, Compos. Sci. Technol. 61 (2001) 837–847.
[18] R. Schueler, S.P. Joshi, K. Schulte, Damage detection in CFRP by electrical conductivity mapping, Compos. Sci. Technol. 61 (2001) 921–930.
[19] N. Angelidis, P.E. Irving, Detection of impact damage in CFRP laminates by means of electrical potential techniques, Compos. Sci. Technol. 67 (2007) 594–604.
[20] L. Bertolini, F. Bolzoni, T. Pastore, P. Pedeferri, Effectiveness of a conductive cementitious mortar anode for cathodic protection of steel in concrete, Cem. Concr. Res. 34 (2004) 681–694.
[21] E. Redaelli, L. Bertolini, Macroscopic observations on the long-term effects of cathodic protection applied to carbonated reinforced concrete, Mater. Corros. 66 (2015) 756–762.
[22] W.H.A. Peelen, R.B. Polder, E. Redaelli, L. Bertolini, Qualitative model of concrete acidification due to cathodic protection, Mater. Corros. 59 (2008) 81–89.
[23] C.J. Mudd, G.L. Mussinelli, M. Tettamanti, P. Pedeferri, Cathodic protection of steel in concrete, Mater. Performance 27 (1988) 18–24.
[24] R.B. Polder, G. Leegwater, D. Worm, W. Courage, Service life and life cycle cost modelling of cathodic protection systems for concrete structures, Cement Concr. Compos. 47 (2014) 69–74.
[25] NACE TM0294, Testing of embeddable impressed current anodes for use in cathodic protection of atmospherically exposed steel-reinforced concrete, 2007.
[26] J.H. Zhu, G. Guo, L. Wei, M. Zhu, X. Chen, Dual Function behavior of carbon fiber-reinforced polymer in simulated pore solution, Materials 9 (2016) 103.
[27] H. Sun, L. Wei, M. Zhu, N. Han, J.H. Zhu, F. Xing, Corrosion behavior of carbon fiber reinforced polymer anode in simulated impressed current cathodic protection system with 3% NaCl solution, Constr. Build. Mater. 112 (2016) 538–546.
[28] ASTM D638, Standard test method for tensile properties of plastics, 2008.
[29] ASTM D1141, Standard practice for the preparation of substitute ocean water, 2008.
[30] NACE SP0290, Impressed current cathodic protection of reinforcing steel in atmospherically exposed concrete structures, 2007.
[31] G. Mussinelli, P. Pedeferri, M. Tettamanti, The effect of current density on anode behaviour and on concrete in the anode region, in: 2nd Int. Conf. Deterioration and Repair of Reinforced Concrete in the Arabian Gulf, Bahrain, 11-13 October 1987.
[32] G.E. Cavigliasso, M.J. Esplandiu, V.A. Macagno, Influence of the forming electrolyte on the electrical properties of tantalum and niobium oxide films: an EIS comparative study, J. Appl. Electrochem. 28 (1998) 1213–1219.
[33] K.V. Subramaniam, M. Bi, Investigation of the local response of the steel–concrete interface for corrosion measurement, Corros. Sci. 51 (2009) 1976–1984.
[34] R.M. Carranza, M.G. Alvarez, The effect of temperature on the passive film properties and pitting behaviour of a Fe-Cr-Ni alloy, Corros. Sci. 38 (1996) 909–925.
[35] G.J. Brug, A.L.G.V.D. Eeden, M. Sluyters-Rehbach, J.H. Sluyters, The analysis of electrode impedances complicated by the presence of a constant phase element, J. Electroanal. Chem. Interfacial Electrochem. 176 (1984) 275–295.
[36] N. Dilsiz, J.P. Wightman, Surface analysis of unsized and sized carbon fibers, Carbon 37 (1999) 1105–1114.
[37] X. Qian, J. Zhi, L. Chen, J. Huang, Y. Zhang, Effect of low current density electrochemical oxidation on the properties of carbon fiber-reinforced epoxy resin composites, Surf. Interface Anal. 45 (2013) 937–942.
[38] S. Osbeck, R.H. Bradley, C. Liu, H. Idriss, S. Ward, Effect of an ultraviolet/ozone treatment on the surface texture and functional groups on polyacrylonitrile carbon fibres, Carbon 49 (2011) 4322–4330.
[39] D.H. Kroon, Cathodic protection anodes underground, Mater. Performance 28 (1989) 17–20.
[40] T. Ueda, J. Dai, Interface bond between FRP sheets and concrete substrates: properties, numerical modeling and roles in member behavior, Prog. Struct. Mat. Eng. 7 (2005) 27–43.
[41] L. Vasseur, S. Matthys, L. Taerwe, An analytical study on the bond behaviour between an externally bonded FRP and concrete in the case of continuous beams, Mech. Compos. Mater. 44 (2008) 269–278.
[42] A. Palmieri, S. Matthys, A.O.B. Joaquim, I. Costa, A. Bilotta, E. Nigro, F. Ceroni, Z. Szambo, G. Balazs, Bond of NSM FRP strengthened concrete: round robin test initiative, in: 6th International Conference on FRP Composites in Civil Engineering, Rome, Italy, 13-15 June 2012, pp. 1-8.